Letter

Emergence of resonating valence-bond correlations in stretched graphene

S. Azadi [1,*] A. Principi [1] T. D. Kühne [2,3,4] and M. S. Bahramy [1]

[1]*Department of Physics and Astronomy, University of Manchester, Oxford Road, Manchester M13 9PL, United Kingdom*

[2]*Center for Advanced Systems Understanding, Untermarkt 20, D-02826 Görlitz, Germany*

[3]*Helmholtz Zentrum Dresden-Rossendorf, Bautzner Landstraße 400, D-01328 Dresden, Germany*

[4]*TU Dresden, Institute of Artificial Intelligence, Chair of Computational System Sciences, Nöthnitzer Straße 46 D-01187 Dresden, Germany*

(Received 30 April 2026; revised 7 July 2026; accepted 10 August 2026; published 24 August 2026)

Electronic correlations in graphene are generally considered weak due to the large bandwidth of its π electrons. Here we show that tensile expansion of the honeycomb lattice provides a direct route to enhancing correlation effects. Using variational and diffusion quantum Monte Carlo, we compare a conventional Jastrow-Slater determinant wave function with a resonating-valence-bond (RVB) Jastrow-antisymmetrized geminal product ansatz for a series of stretched graphene lattices. We find that the energy gain of the RVB state relative to the single-determinant description increases with bond expansion up to a critical strain δ_{cr}, and decreases beyond it, revealing a nonmonotonic evolution of electronic correlations. A quantitative analysis places $\delta_{\mathrm{cr}} \approx 14$–$19\%$ across the system sizes studied, extrapolating to $13.7 \pm 0.8\%$ in the thermodynamic limit. Analysis of the optimized many-body pairing amplitude further reveals that this crossover is accompanied by a sharp, specific enhancement of π-orbital character in the nearest-neighbor pairing between adjacent carbon atoms, providing direct microscopic evidence for the emergence of RVB-like bonding. This behavior indicates a transition from a weakly correlated Dirac semimetal to a regime with enhanced nondynamic correlation and short-range singlet pairing. Our results provide direct many-body evidence that lattice expansion drives graphene into a regime where RVB-like correlations become energetically favorable, offering a simple route to tuning correlation effects in Dirac materials.

DOI: 10.1103/96cl-xq62

Introduction. Graphene provides a unique platform for exploring the interplay between lattice geometry and electronic correlation in low-dimensional systems [1–10]. In its equilibrium structure, the π-electrons form a wide-band Dirac semimetal, where the large hopping amplitude between neighboring p_z orbitals leads to highly delocalized electronic states and relatively weak correlation effects. However, the strength of electronic correlations in such systems is not fixed, but can be tuned by modifying the balance between kinetic energy and Coulomb interactions. In particular, tensile expansion of the graphene lattice increases the C–C bond length, thereby reducing the orbital overlap and suppressing the hopping amplitude that controls the electronic bandwidth. Within this picture, lattice stretching effectively enhances the relative importance of electron-electron interactions and drives the system toward a more strongly correlated regime. Understanding how the electronic ground state evolves under such conditions is therefore of fundamental interest, as it provides insight into the emergence of correlation-driven phenomena in Dirac materials and related honeycomb lattices.

The effect of tensile strain on graphene [11] has been studied at the level of elasticity and band structure. First-principles calculations and experiments have established that ideal monolayer graphene sustains large tensile deformation, with biaxial instability occurring at strains of order 15–20% [12–14]. Within tight-binding descriptions, strain primarily reduces the nearest-neighbor hopping amplitude, leading to modifications of the Dirac spectrum and a suppression of the electronic bandwidth [3,5,15]. This bandwidth reduction has been proposed as a route to enhancing interaction effects, for example, by bringing van Hove singularities closer to the Fermi level and promoting correlation-driven instabilities [16–18]. In parallel, the half-filled Hubbard model on the honeycomb lattice has provided a paradigmatic framework for understanding correlation effects in graphene, predicting a transition from a Dirac semimetal to an antiferromagnetic insulator with increasing effective interaction strength U/t [19–21]. While these studies suggest that lattice expansion can drive graphene toward a strongly correlated regime, a direct parameter free *ab initio* many-body characterization of how electronic correlations evolve under controlled bond stretching remains largely unexplored.

Quantum Monte Carlo (QMC) methods [22–25] have become one of the most accurate and systematically improvable approaches for describing electronic correlation in real materials. In particular, variational and diffusion Monte Carlo calculations based on the conventional Jastrow-Slater determinant (JSD) wave function have demonstrated remarkable

*Contact author: sam.azadi@manchester.ac.uk

Published by the American Physical Society under the terms of the Creative Commons Attribution 4.0 International license. Further distribution of this work must maintain attribution to the author(s) and the published article's title, journal citation, and DOI.

success in capturing correlation effects. The Jastrow factor efficiently incorporates short-range electron-electron and electron-nucleus correlations, substantially improving the description of many-body effects while preserving the fermionic antisymmetry through the Slater determinant. This framework has been successfully applied to a wide range of systems, including bulk solids [26–30], molecular structures [31–33], and low-dimensional materials [34–37], providing highly accurate ground-state energies, cohesive energies, and structural properties. In particular, QMC calculations using JSD wave functions have proven effective for two-dimensional systems such as graphene and other layered materials, where reduced dimensionality enhances correlation effects.

However, the accuracy of a single SD description can deteriorate when the interatomic distance in a system increases. As the overlap between neighboring orbitals decreases, the electronic kinetic energy is reduced and the system approaches a regime where the static correlation effects become important. A typical manifestation of this behavior is observed in bond stretching, where the correct description of the electronic state requires a superposition of multiple configurations to account for the partial localization of electrons and the formation of correlated singlet pairs. Within QMC, these effects cannot be fully captured by the conventional JSD wave function. A more flexible alternative is provided by the antisymmetrized geminal product (AGP) ansatz, in which the wave function is constructed from correlated electron pairs rather than independent single-particle orbitals. When combined with a Jastrow factor, the resulting Jastrow-AGP (JAGP) form naturally incorporates multideterminant character and provides an efficient description of static correlation and resonating valence-bond (RVB) [38–45] like pairing correlations in extended systems.

This work deploys real-space variational quantum Monte Carlo (VMC) and diffusion quantum Monte Carlo (DMC) methods [46–57] combined with density functional theory (DFT) [58–60] to elucidate the effect of isotropic biaxial strain on the many-body Coulomb interaction between electrons and single-particle spectra of graphene. We investigate the evolution of electronic correlations in graphene under controlled bond expansion. In VMC, expectation values are computed by sampling a parametrized trial wave function in real space, JSD, and JAGP in this work, and optimizing its parameters to minimize the variational energy. The accuracy of VMC is therefore determined by the flexibility of the chosen ansatz and the quality of its nodal structure. DMC goes beyond this by projecting the trial wave function onto the ground state through an imaginary-time evolution of the Schrödinger equation, effectively filtering out higher-energy components. In practice, DMC is implemented with the fixed-node approximation [61], which constrains the nodal surface to that of the trial wave function, making the resulting energy an upper bound to the exact ground-state energy within this constraint. Details of DFT and QMC calculations, together with the full statistical analysis underlying the quantitative results below, are provided in the Supplemental Material [62].

By comparing the energies obtained with a JSD wave function and a JAGP ansatz, we directly quantify the role of static many-body correlation embedded in JAGP as a function of isotropic biaxial stretch. We find that the energy gain of

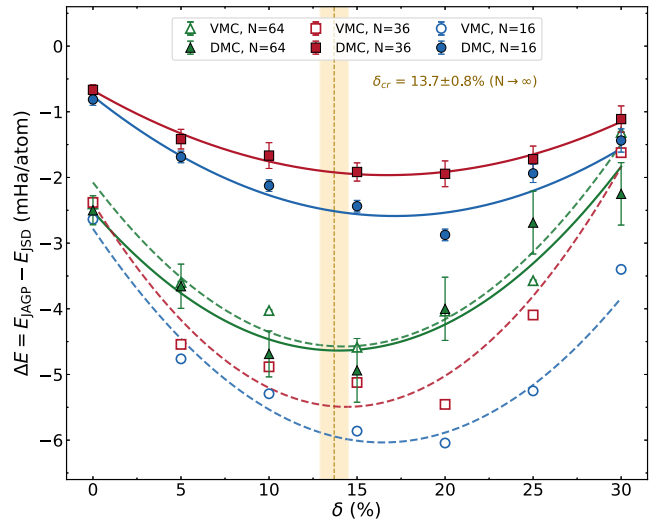


FIG. 1. Energy difference $\Delta E = E_{\mathrm{JAGP}} - E_{\mathrm{JSD}}$ per atom as a function of in-plane biaxial strain δ, obtained from VMC (open symbols, dashed lines) and DMC (filled symbols, solid lines) calculations for system sizes $N = 16, 36, 64$. Lines are weighted quadratic fits to each data set (Supplemental Material [62]). The shaded band marks the critical strain $\delta_{\mathrm{cr}} = 13.7 \pm 0.8\%$ extrapolated to the thermodynamic limit $N \to \infty$. The nonmonotonic behavior reflects the enhancement of static, RVB-like singlet correlations up to δ_{cr}, followed by a crossover to a different correlation regime at larger strain.

the JAGP wave function increases with bond stretching up to a critical strain δ_{cr}, and decreases beyond it, revealing a nonmonotonic evolution of correlation effects. These results indicate that tensile expansion drives graphene from a weakly correlated Dirac semimetal into a regime with enhanced RVB-like correlations, with maximal pairing character at intermediate bond expansion.

The VMC and DMC energies obtained with both JSD and JAGP wave functions for system sizes of $N = 16$, 36, and 64 atoms show a systematic increase in total energy with increasing lattice expansion δ (Fig. 1). As expected, the equilibrium configuration at $\delta = 0$ corresponds to the minimum energy for all system sizes and wave-function ansatz. The energy difference between JAGP and JSD wave functions provides a measure of the pairing component of the electronic correlation energy. We find the same qualitative nonmonotonic trend at both levels of theory, and already at the level of the trial wave function in VMC, indicating it is not an artifact of DMC projection. The observed increase in the magnitude of $E_{\mathrm{JAGP}} - E_{\mathrm{JSD}}$ with bond expansion up to δ_{cr} indicates RVB-like singlet correlations. This behavior is consistent with a bandwidth-controlled increase of static correlation in the honeycomb lattice. However, the subsequent reduction of the JAGP energy gain at larger expansion signals a qualitative change in the nature of the correlated ground state. This nonmonotonic behavior suggests a crossover from an itinerant regime with enhanced singlet pairing correlations to a regime in which localization or alternative correlation mechanisms become dominant. Our results therefore demonstrate that tensile expansion does not simply strengthen electronic correlations, but drives a transition between distinct correlated

regimes, with RVB-like correlations maximized at intermediate bond lengths.

The magnitude of the energy gain obtained with the JAGP wave function relative to JSD, in both VMC and DMC calculations, increases with lattice expansion up to a critical strain δ_{cr}, after which it decreases. A quantitative analysis of this nonmonotonic behavior—weighted quadratic and quartic fits to $\Delta E(\delta)$ at each system size, validated against each other by a nested F-test, together with a finite-size extrapolation in $1/N$—places $\delta_{\mathrm{cr}} \approx 14$–$19\%$ across $N = 16, 36, 64$, extrapolating to $13.7 \pm 0.8\%$ in the thermodynamic limit (full statistical analysis in the Supplemental Material [62]). This trend indicates that tensile expansion enhances the importance of static, multiconfigurational correlation, which is efficiently captured by the singlet pairing structure of the JAGP ansatz. We further determined the mechanical (spinodal) instability strain directly at the QMC level, independent of any DFT-level elastic-constant calculation, from the inflection point of the same DMC total-energy curves, obtaining ≈ 21–22% at our largest system size—several percentage points above δ_{cr}. RVB-like correlations are therefore maximized while the lattice is approaching, but has not yet reached, mechanical failure, rather than precisely at the instability threshold. In this region, the reduction of orbital overlap and the resul of ting near-degeneracy of electronic configurations render a single-determinant description increasingly inadequate, while correlated singlet pairing provides a more favorable description of the ground state. These results therefore indicate that electronic correlation plays a significant role in stabilizing the stretched bonded state, lowering its energy relative to a single-determinant picture, and that the approach to mechanical instability occurs in a regime where many-body effects are already strongly enhanced.

The DFT electronic structure of graphene is characterized by a clear separation between π and σ bands [62]. The bands forming the Dirac cones at the K points originate from p_z-derived π and π^* states, while the saddle point at M is also associated with the same π-band. In contrast, states near the Γ point are dominated by in-plane σ and σ^* bands derived from sp^2 orbitals, with a gap separating valence and conduction branches. Along the Γ-K and Γ-M directions, the π^* and σ^* conduction bands can cross due to their distinct symmetry under mirror reflection with respect to the graphene plane, which suppresses hybridization between out-of-plane and in-plane states.

The DFT band structures under isotropic in-plane tensile expansion show that the primary effect of strain is a strong renormalization of the conduction manifold, while the low-energy Dirac physics remains intact [62]. The degeneracy among conduction bands is lifted by δ, and the conduction π^* and σ^* bands shift toward the Fermi level as the C–C bond length increases. In contrast, the Dirac crossing at the K point is preserved exactly (the gap at K vanishes to machine precision at every strain studied), consistent with the maintained lattice symmetry under biaxial strain. The Fermi velocity at K decreases steadily with strain, from 0.79×10^6 m/s at $\delta = 5\%$ to 0.53×10^6 m/s at $\delta = 30\%$—a $\approx$33% reduction consistent with a simple tight-binding estimate and with the experimentally reported range for unstrained graphene once the expected strain suppression is accounted for (Supplemental Material [62]). A flattening of the π^* band is observed prior to its crossing with the σ^* band along the Γ-K and Γ-M directions, indicating a reduction of the effective kinetic energy scale; correspondingly, the gap between the two lowest conduction bands at M closes by more than an order of magnitude with strain, from 4.47 eV at $\delta = 5\%$ to 0.36 eV at $\delta = 30\%$. In addition, the bonding-antibonding splitting within the in-plane σ bands decreases, leading to a reduction of the valence-conduction gap at the Γ point. The DFT band structure results indicate a systematic suppression of orbital overlap and bandwidth under increasing δ.

These single-particle trends provide a direct interpretation of the QMC results. The flattening of the π^* band and the reduction of antibonding splittings imply a decrease in the hopping amplitude, and hence, an increase in the effective interaction-to-bandwidth ratio. This is consistent with the observed increase in the energy gain of the JAGP wave function relative to JSD up to intermediate strain, indicating the growing importance of nondynamic correlation and short-range singlet pairing. The subsequent reduction of this energy gain at larger expansion correlates with the continued shift and restructuring of the conduction bands, suggesting a crossover from a regime dominated by delocalized RVB-like correlations to one where changes in the orbital character of the low-energy excitations modify the nature of the correlated ground state—a picture we confirm directly, at the level of the many-body pairing amplitude itself, below.

The projected density of states (pDOS) provides a consistent spectral interpretation of the strain-dependent band structure [62]. The p_z-resolved DOS shows that the van Hove singularities associated with the π bands are preserved under tensile expansion, but become narrower and move closer in energy, reflecting a reduction of bandwidth and band flattening without opening a gap at the Fermi level. At the same time, the $s + p_x + p_y$-projected DOS reveals that the antibonding σ^* states shift toward lower energies and gain weight above the Fermi level, reducing the bonding-antibonding splitting within the σ band. This leads to a decrease of the σ–σ^* gap at Γ and an increasing energetic proximity between π^* and σ^* states, in agreement with the band structure. The DOS confirms that tensile strain primarily suppresses the kinetic energy scale and compresses the conduction spectrum while preserving the gapless Dirac character of graphene.

To connect this single-particle picture directly to the many-body wave function, we analyze the real-space structure of the optimized JAGP pairing amplitude at our largest system size ($N = 64$). For each pair of atoms a, b we define $\|\Lambda_{ab}\| = (\sum_{i\in a, j\in b} \lambda_{ij}^2)^{1/2}$, the aggregate weight of the geminal matrix connecting all atomic orbitals on atom a to those on atom b; a companion JSD calculation contributes identically zero weight in this same atomic-orbital basis, so this quantity captures precisely the additional pairing structure JAGP introduces relative to JSD. This pairing amplitude decays rapidly and monotonically with inter-atomic distance at every strain studied [Fig. 2(a)], falling to roughly half its on-site value within one bond length and to a fifth or less within three bond lengths, the real-space signature of short-range, RVB-like singlet pairing rather than a long-range paired state.

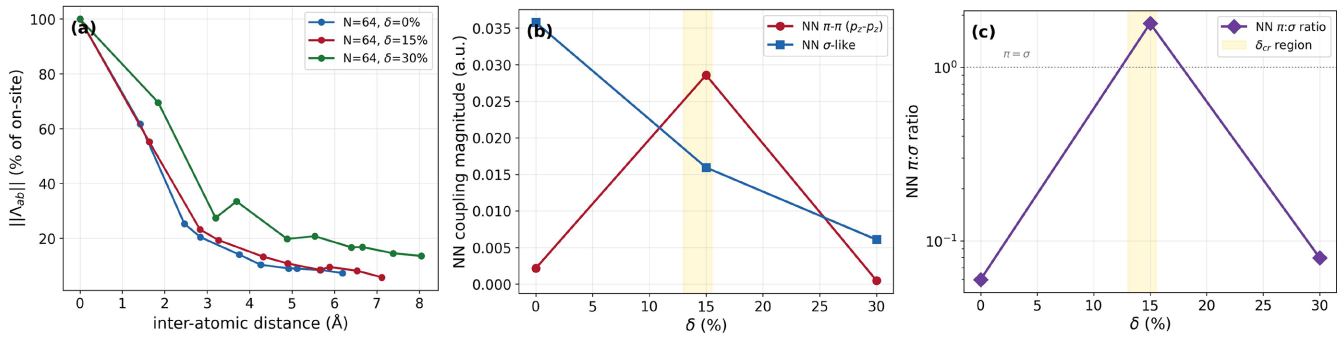


FIG. 2. (a) Real-space decay of the JAGP pairing amplitude $\|\Lambda_{ab}\|$ with interatomic distance, for $N = 64$ at $\delta = 0, 15, 30\%$. (b) Nearest-neighbor (NN) π-channel (p_z-p_z) and σ-like (in-plane p_x, p_y) coupling magnitude versus strain. (c) The corresponding NN π:σ ratio, on a logarithmic scale; the shaded band marks $\delta_{\rm cr}$, where the ratio crosses unity.

Resolving this pairing amplitude by orbital character reveals a more specific picture. Because of the relevant physics, bandwidth narrowing under strain and the π^*-σ^* band crossing discussed above, is an inherently interatomic, bonding phenomenon, we examine the π-channel (p_z-p_z) and σ-like (in-plane p_x, p_y) coupling between each atom and its three nearest neighbors [Figs. 2(b) and 2(c)]. At equilibrium and at $\delta = 30\%$, the nearest-neighbor coupling is σ-dominated, exceeding the π coupling by more than an order of magnitude. At $\delta \approx 15\%$, close to $\delta_{\rm cr}$, this reverses sharply as the π-channel coupling exceeds the σ-like coupling by a factor of $\approx$1.8 indicating a crossover in nearest-neighbor bonding character. This provides direct, bond-resolved microscopic evidence that the correlation-energy peak at $\delta_{\rm cr}$ coincides with the RVB-like pairing becoming preferentially π-bond-dominated between neighboring atoms, consistent with the reduced Fermi velocity, the closing gap at M, and the flattening of the π^* band established above. This real-space pairing amplitude, by construction, characterizes the magnitude of short-range singlet correlations but does not by itself distinguish genuine RVB coverage from an antiferromagnetic (Néel) precursor, both of which produce short-range singlet correlations of this general form; a rigorous determination requires the spin-spin correlation function, which we leave to a dedicated follow-up study.

Although increasing the lattice expansion δ enhances static correlation in graphene, particularly at intermediate C–C bond lengths, this effect cannot be mapped directly onto the single-parameter Hubbard model on the honeycomb lattice. In the latter, increasing U/t drives a well-defined transition from a Dirac semimetal to an antiferromagnetic insulating state, with no stable spin-liquid phase [20,63]. In contrast, tensile expansion in graphene modifies not only the effective hopping amplitude but also the full band structure and orbital energetics. As a result, δ does not provide a one-to-one correspondence with U/t, and the evolution of correlation in the stretched lattice cannot be interpreted within a simple Hubbard framework. The present results therefore highlight that, while the honeycomb Hubbard model offers useful qualitative insight, a quantitative connection between lattice models and first-principles many-body calculations requires a more detailed mapping that accounts for multiorbital effects and long-range interactions.

In this work, we investigate the evolution of electronic correlations in graphene under isotropic tensile expansion using a combination of DFT and QMC methods. The DFT band structures and pDOS show that strain preserves the gapless Dirac spectrum while strongly renormalizing the conduction band, leading to band flattening, reduced antibonding splittings, and a compression of the energy scale associated with both π^* and σ^* states. These single-particle effects indicate a systematic reduction of the kinetic energy scale with increasing C–C bond length.

The QMC results provide direct many-body evidence of how these changes impact electronic correlation. The increasing energy gain of the JAGP wave function relative to the JSD up to intermediate strain demonstrates the growing importance of static, multiconfigurational correlation and short-range singlet pairing, with a critical strain $\delta_{\rm cr} \approx 14$–$19\%$ (extrapolating to $13.7 \pm 0.8\%$ as $N \to \infty$) that precedes the QMC-determined mechanical instability threshold ($\approx$ 21–22%). The subsequent reduction of this gain at larger expansion reveals a nonmonotonic evolution of correlation effects, indicating a crossover between distinct correlation regimes. A direct, real-space analysis of the optimized pairing amplitude confirms this picture at the orbital level, revealing a sharp crossover from σ- to π-dominated nearest-neighbor bonding character precisely in the vicinity of $\delta_{\rm cr}$. These findings show that tensile expansion does not simply enhance correlation in a uniform manner, but instead drives the system toward a regime where RVB-like correlations, and specifically π-channel singlet pairing, are maximized before further evolution toward a different, more σ-dominated correlated state.

Acknowledgments. We acknowledge the support of the Leverhulme Trust under the Grant Agreement No. RPG-2023-253. S.A. and T.D.K. acknowledge the computing time provided to them on the high-performance computers Noctua2 at the NHR Center in Paderborn (PC2).

Data availability. The data that support the findings of this article are openly available [64].

[1] K. Novoselov, A. Geim, S. Morozov, D. Jiang, Y. Zhang, S. Dubonos, I. Grigorieva, and A. Firsov, Electric field effect in atomically thin carbon films, Science **306**, 666 (2004).

[2] A. Geim and K. Novoselov, The rise of graphene, Nat. Mater. **6**, 183 (2007).

[3] A. H. C. Neto, F. Guinea, N. M. R. Peres, K. S. Novoselov, and A. K. Geim, The electronic properties of graphene, Rev. Mod. Phys. **81**, 109 (2009).

[4] K. Novoselov, A. Geim, S. V. Morozov, D. Jiang, M. I. Katsnelson, I. Grigorieva, S. Dubonos, and A. Firsov, Two-dimensional gas of massless Dirac fermions in graphene, Nature (London) **438**, 197 (2005).

[5] V. N. Kotov, B. Uchoa, V. M. Pereira, F. Guinea, and A. H. Castro Neto, Electron-electron interactions in graphene: Current status and perspectives, Rev. Mod. Phys. **84**, 1067 (2012).

[6] S. D. Sarma, S. Adam, E. H. Hwang, and E. Rossi, Electronic transport in two-dimensional graphene, Rev. Mod. Phys. **83**, 407 (2011).

[7] Y. Cao, V. Fatemi, S. Fang, K. Watanabe, T. Taniguchi, E. Kaxiras, and P. Jarillo-Herrero, Unconventional superconductivity in magic-angle graphene superlattices, Nature (London) **556**, 43 (2018).

[8] H. Zheng, Y. Gan, P. Abbamonte, and L. K. Wagner, Importance of σ bonding electrons for the accurate description of electron correlation in graphene, Phys. Rev. Lett. **119**, 166402 (2017).

[9] I. F. Herbut, Interactions and phase transitions on graphene's honeycomb lattice, Phys. Rev. Lett. **97**, 146401 (2006).

[10] I. F. Herbut, V. Juricic, and B. Roy, Theory of interacting electrons on the honeycomb lattice, Phys. Rev. B **79**, 085116 (2009).

[11] F. Guinea, M. Katsnelson, and A. Geim, Energy gaps and a zero-field quantum Hall effect in graphene by strain engineering, Nat. Phys. **6**, 30 (2010).

[12] G. J. Verbiest, C. Stampfer, S. E. Huber, M. Andersen, and K. Reuter, Interplay between nanometer-scale strain variations and externally applied strain in graphene, Phys. Rev. B **93**, 195438 (2016).

[13] B. Rakshit and P. Mahadevan, Absence of rippling in graphene under biaxial tensile strain, Phys. Rev. B **82**, 153407 (2010).

[14] L. Changgu, X. Wei, J. Kysar, and J. Hone, Measurement of the elastic properties and intrinsic strength of monolayer graphene, Science **321**, 385 (2008).

[15] V. M. Pereira, A. H. Castro Neto, and N. M. R. Peres, Tight-binding approach to uniaxial strain in graphene, Phys. Rev. B **80**, 045401 (2009).

[16] B. Uchoa and A. H. Castro Neto, Superconducting states of pure and doped graphene, Phys. Rev. Lett. **98**, 146801 (2007).

[17] J. L. McChesney, A. Bostwick, T. Ohta, T. Seyller, K. Horn, J. Gonzalez, and E. Rotenberg, Extended Van Hove singularity and superconducting instability in doped graphene, Phys. Rev. Lett. **104**, 136803 (2010).

[18] S. Pathak, V. B. Shenoy, and G. Baskaran, Possible high-temperature superconducting state with a $d + id$ pairing symmetry in doped graphene, Phys. Rev. B **81**, 085431 (2010).

[19] T. Paiva, R. T. Scalettar, W. Zheng, R. R. P. Singh, and J. Oitmaa, Ground-state and finite-temperature signatures of quantum phase transitions in the half-filled Hubbard model on a honeycomb lattice, Phys. Rev. B **72**, 085123 (2005).

[20] S. Sorella, Y. Otsuka, and S. Yunoki, Absence of a spin liquid phase in the Hubbard model on the honeycomb lattice, Sci. Rep. **2**, 992 (2012).

[21] F. F. Assaad and I. F. Herbut, Pinning the order: The nature of quantum criticality in the Hubbard model on honeycomb lattice, Phys. Rev. X **3**, 031010 (2013).

[22] D. Ceperley, G. V. Chester, and M. H. Kalos, Monte Carlo simulation of a many-fermion study, Phys. Rev. B **16**, 3081 (1977).

[23] D. Ceperley and B. Alder, Quantum Monte Carlo, Science **231**, 555 (1986).

[24] W. M. C. Foulkes, L. Mitas, R. J. Needs, and G. Rajagopal, Quantum Monte Carlo simulations of solids, Rev. Mod. Phys. **73**, 33 (2001).

[25] F. Becca and S. Sorella, *Quantum Monte Carlo Approches for Correlated Systems* (Cambridge University, Cambridge, England, 2017).

[26] N. D. Drummond, M. D. Towler, and R. J. Needs, Jastrow correlation factor for atoms, molecules, and solids, Phys. Rev. B **70**, 235119 (2004).

[27] N. D. Drummond, A. J. Williamson, R. J. Needs, and G. Galli, Electron emission from diamondoids: A diffusion quantum Monte Carlo study, Phys. Rev. Lett. **95**, 096801 (2005).

[28] J. Kolorenč and L. Mitas, Applications of quantum Monte Carlo methods in condensed systems, Rep. Prog. Phys. **74**, 026502 (2011).

[29] K. Foyevtsova, J. T. Krogel, J. Kim, P. R. C. Kent, E. Dagotto, and F. A. Reboredo, *Ab initio* quantum Monte Carlo calculations of spin superexchange in cuprates: The benchmarking case of Ca_2CuO_3, Phys. Rev. X **4**, 031003 (2014).

[30] S. Azadi, N. D. Drummond, A. Principi, R. V. Belosludov, and M. S. Bahramy, Quantum Monte Carlo study of the quasiparticle effective mass of the two-dimensional uniform electron liquid, Phys. Rev. B **112**, 075141 (2025).

[31] A. Zen, J. G. Brandenburg, J. Klimes, A. Tkatchenko, D. Alfe, and A. Michaelides, Fast and accurate quantum Monte Carlo for molecular crystals, Proc. Natl. Acad. Sci. USA **115**, 1724 (2018).

[32] G. Mazzola, S. Yunoki, and S. Sorella, Unexpectedly high pressure for molecular dissociation in liquid hydrogen by electronic simulation, Nat. Commun. **5**, 3487 (2014).

[33] S. Sorella, M. Casula, and D. Rocca, Weak binding between two aromatic rings: Feeling the van der Waals attraction by quantum Monte Carlo methods, J. Chem. Phys. **127**, 014105 (2007).

[34] E. Mostaani, N. D. Drummond, and V. I. Falko, Quantum Monte Carlo calculation of the binding energy of bilayer graphene, Phys. Rev. Lett. **115**, 115501 (2015).

[35] E. Mostaani, M. Szyniszewski, C. H. Price, R. Maezono, M. Danovich, R. J. Hunt, N. D. Drummond, and V. I. Falko, Diffusion quantum Monte Carlo study of excitonic complexes in two-dimensional transition-metal dichalcogenides, Phys. Rev. B **96**, 075431 (2017).

[36] L. Spanu, S. Sorella, and G. Galli, Nature and strength of interlayer binding in graphite, Phys. Rev. Lett. **103**, 196401 (2009).

[37] S. Azadi, A. Principi, T. D. Kühne, and M. S. Bahramy, Resonating valence bond pairing energy in graphene by quantum Monte Carlo, Phys. Rev. B **113**, L121101 (2026).

[38] L. Pauling, *The Nature of the Chemical Bond* (Cornell University Press, Ithaca, NY, 1960).

[39] P. W. Anderson, The resonating valence bond state in La_2CuO_4 and superconductivity, Science **235**, 1196 (1987).
[40] L. Capriotti, F. Becca, A. Parola, and S. Sorella, Resonating valence bond wave functions for strongly frustrated spin systems, Phys. Rev. Lett. **87**, 097201 (2001).
[41] P. W. Anderson, G. Baskaran, Z. Zou, and T. Hsu, Resonating–valence-bond theory of phase transitions and superconductivity in La_2CuO_4-based compounds, Phys. Rev. Lett. **58**, 2790 (1987).
[42] G. Baskaran, Electronic model for CoO_2 layer based systems: Chiral resonating valence bond metal and superconductivity, Phys. Rev. Lett. **91**, 097003 (2003).
[43] S. A. Kivelson, I. P. Bindloss, E. Fradkin, V. Oganesyan, J. M. Tranquada, A. Kapitulnik, and C. Howald, How to detect fluctuating stripes in the high-temperature superconductors, Rev. Mod. Phys. **75**, 1201 (2003).
[44] A. M. Black-Schaffer and S. Doniach, Resonating valence bonds and mean-field *d*-wave superconductivity in graphite, Phys. Rev. B **75**, 134512 (2007).
[45] S. Azadi, R. Singh, and T. D. Kühne, Resonating valence bond Quantum Monte Carlo: Application to the ozone molecule, Int. J. Quantum Chem. **115**, 1673 (2015).
[46] K. Nakano, C. Attaccalite, M. Barborini, L. Capriotti, M. Casula, E. Coccia, M. Dagrada, C. Genovese, Y. Luo, G. Mazzola, A. Zen, and S. Sorella, Turborvb: A many-body toolkit for *ab initio* electronic simulations by quantum Monte Carlo, J. Chem. Phys. **152**, 204121 (2020).
[47] M. Marchi, S. Azadi, M. Casula, and S. Sorella, Resonating valence bond wave function with molecular orbitals: Application to first-row molecules, J. Chem. Phys. **131**, 154116 (2009).
[48] M. Marchi, S. Azadi, and S. Sorella, Fate of the resonating valence bond in graphene, Phys. Rev. Lett. **107**, 086807 (2011).
[49] A. Annaberdiyev, G. Wang, C. A. Melton, M. C. Bennett, L. Shulenburger, and L. Mitas, A new generation of effective core potentials from correlated calculations: 3d transition metal series, J. Chem. Phys. **149**, 134108 (2018).
[50] M. C. Bennett, C. A. Melton, A. Annaberdiyev, G. Wang, L. Shulenburger, and L. Mitas, A new generation of effective core potentials for correlated calculations, J. Chem. Phys. **147**, 224106 (2017).
[51] J. P. Perdew and A. Zunger, Self-interaction correction to density-functional approximations for many-electron systems, Phys. Rev. B **23**, 5048 (1981).
[52] S. Azadi, C. Cavazzoni, and S. Sorella, Systematically convergent method for accurate total energy calculations with localized atomic orbitals, Phys. Rev. B **82**, 125112 (2010).
[53] S. Fahy, X. W. Wang, and S. G. Louie, Variational quantum Monte Carlo nonlocal pseudopotential approach to solids: Formulation and application to diamond, graphite, and silicon, Phys. Rev. B **42**, 3503 (1990).
[54] C. J. Umrigar, J. Toulouse, C. Filippi, S. Sorella, and R. G. Hennig, Alleviation of the fermion-sign problem by optimization of many-body wave functions, Phys. Rev. Lett. **98**, 110201 (2007).
[55] S. Sorella, Green function Monte Carlo with stochastic reconfiguration, Phys. Rev. Lett. **80**, 4558 (1998).
[56] M. Casula, Beyond the locality approximation in the standard diffusion Monte Carlo method, Phys. Rev. B **74**, 161102(R) (2006).
[57] S. Sorella, Wave function optimization in the variational Monte Carlo method, Phys. Rev. B **71**, 241103(R) (2005).
[58] P. Giannozzi *et al.*, QUANTUM ESPRESSO: A modular and open-source software project for quantum simulations of materials, J. Phys.: Condens. Matter **21**, 395502 (2009).
[59] P. Giannozzi *et al.*, Advanced capabilities for materials modelling with QUANTUM ESPRESSO, J. Phys.: Condens. Matter **29**, 465901 (2017).
[60] J. P. Perdew, K. Burke, and M. Ernzerhof, Generalized gradient approximation made simple, Phys. Rev. Lett. **77**, 3865 (1996).
[61] L. Mitas, Structure of fermion nodes and nodal cells, Phys. Rev. Lett. **96**, 240402 (2006).
[62] See Supplemental Material at http://link.aps.org/supplemental/10.1103/96cl-xq62 for details of our QMC and DFT calculations, additional figures, and data.
[63] S. Sorella and E. Tosatti, Semi-metal-insulator transition of the Hubbard model in the honeycomb lattice, Europhys. Lett. **19**, 699 (1992).
[64] S. Azadi, Github, https://github.com/arshamsam.